Effect of mixed Frenkel and charge transfer states in time-gated fluorescence spectra of perylene bisimides H-aggregates: Hierarchical equations of motion approach

Mauro Cainelli, Raffaele Borrelli and Yoshitaka Tanimura

COLLECTIONS

View Online   Export Citation   CrossMark

ARTICLES YOU MAY BE INTERESTED IN

Renormalization of excitonic properties by polar phonons
The Journal of Chemical Physics **157**, 104116 (2022); https://doi.org/10.1063/5.0100738

Numerically "exact" approach to open quantum dynamics: The hierarchical equations of motion (HEOM)
The Journal of Chemical Physics **153**, 020901 (2020); https://doi.org/10.1063/5.0011599

Quantum dynamical study of inter-chain exciton transport in a regioregular P3HT model system at finite temperature: HJ vs H-aggregate models
The Journal of Chemical Physics **157**, 094108 (2022); https://doi.org/10.1063/5.0104729

Effect of mixed Frenkel and charge transfer states in time-gated fluorescence spectra of perylene bisimides H-aggregates: Hierarchical equations of motion approach

Mauro Cainelli,[1,a] (iD) **Raffaele Borrelli,**[1,2,a] (iD) **and Yoshitaka Tanimura**[1,a] (iD)

AFFILIATIONS

[1] Department of Chemistry, Graduate School of Science, Kyoto University, Kyoto 606-8502, Japan
[2] DISAFA, University of Torino, Largo Paolo Braccini 2, I-10095 Grugliasco, Italy

Note: This paper is part of the JCP Special Topic on Photophysics in Emerging Photovoltaics.
[a]**Authors to whom correspondence should be addressed:** cainelli.mauro@gmail.com; raffaele.borrelli@unito.it; and tanimura.yoshitaka.5w@kyoto-u.jp

ABSTRACT

We theoretically investigated the effect of mixed Frenkel (F) and charge transfer (CT) states on the spectral properties of perylene bisimide (PBI) derivatives, focusing on the role of strong electron–phonon interactions. The model consists of a four-level system described by the Holstein Hamiltonian coupled to independent local heat-baths on each site, described by Brownian spectral distribution functions. We employ the reduced hierarchical equations of motion (HEOM) approach to calculate the time evolution of the system and compare it to the pure F exciton cases. We compute the absorption and time-gated fluorescence (TGF) spectra for different exciton transfer integrals and F-CT bandgap conditions. The coherence length of excitons (N_{coh}) is evaluated employing two different definitions. We observe the presence of an excited hot state peak whose intensity is associated with the delocalization of the excited species and ultrafast dynamics that are solely dependent on the frequency of the local bath. The results indicate that the inclusion of CT states promotes localization of the excitons, which is manifested in a decrease in the intensity of the hot state peak and the 0–1 peak and an increase in the intensity of the 0–0 emission peak in the TGF spectrum, leading to a decrease of N_{coh}.

Published under an exclusive license by AIP Publishing. https://doi.org/10.1063/5.0102000

I. INTRODUCTION

Over the past few decades, the development of more efficient photovoltaic devices has been of great interest in the investigation of renewable energy sources. In particular, organic solar cells have proven to be very promising because of their lower manufacturing costs, lighter weight, and greater design flexibility compared to existing silicon-based materials.[1,2] For this reason, several groups have been studying different types of compounds that could be used as donors and acceptors, such as oligoacenes and fullerene/non-fullerene derivatives,[3] respectively, to increase the power conversion efficiency. In this regard, perylene bisimides (PBI) derivatives, which are conjugated molecules that form varieties of π–π stacked H-aggregates, are promising candidates as

semiconductors because of their high photostability and excellent spectral properties, including the ability to change absorption bands by changing substituents.[4,5]

However, the mechanism of photocurrent generation in organic devices is more complex than in their inorganic counterparts, mainly because of the vibronic effect associated with strong electron–phonon interactions.[6,7] Recently, the importance of the inclusion of charge transfer (CT) states and the interaction with Frenkel (F) states on the exciton dynamics of certain systems have been recognized.[8–12] In particular, in systems where this interaction is strong, the Frenkel approximation alone cannot accurately reproduce certain optical properties.[13,14] In such situations, quantum coherence (entanglement) between electrons and phonons is critical in determining the conversion efficiency of the system, and

a quantum-mechanically accurate method describing the strong system-bath interaction must be employed to study the vibronic dynamics on ultrafast time scales.[15] Indeed, some studies have shown that localization processes competing with energy transfer can effectively occur on such ultrafast time scales;[16–18] however, direct experimental results are still needed. Furthermore, while there have been numerous theoretical studies in this area based on approximate theories,[19] no analysis of this type of system using a numerically rigorous approach such as the hierarchical equation of motion (HEOM) has yet been found.

Absorption and photoluminescence (PL) spectra can provide indirect information about the dynamics of the electronic excitation in molecular aggregates, as they depend on the vibronic coupling, and on their effect of spatial coherence.[20–24] More specifically, the coherence length (N_{coh}) has been widely employed as a parameter to evaluate the exciton delocalization,[25,26] and a method was proposed to determine it from the ratio of the 0–0 and 0–1 fluorescence peaks.[27] This method is currently believed to accurately evaluate the N_{coh} value of J-aggregates.[28] Femtosecond time-gated fluorescence (TGF) measurements have been recently used to investigate the dynamics of the delocalization process of PBI H-aggregates,[29] but recent theoretical analyses suggest that, in these systems, this approach may only work for very short time scales.[30] Furthermore, the limitation of the time-gate available to obtain TGF spectra makes it difficult to analyze the exciton dynamics behavior at short times (ultrafast dynamics), which may be important to elucidate the role of the vibronic interactions with high-frequency vibrational modes. Yet, TGF measurements appear to be a very promising tool for investigating the dynamics of exciton delocalization due to their inherently simple physical description.[31–33] Analysis of the commonly obtained pump–probe spectrum for molecular aggregates is much more complex than the emission spectrum because of the contribution of the excited-state absorption (ESA), which is difficult to predict with theoretical calculations. Using the HEOM approach, the TGF spectrum can be theoretically obtained for any time-gate (t_G), providing insight into the vibronic effects on N_{coh}.

The purpose of this paper is to develop a model for the exciton dynamics in PBI aggregates using the HEOM formalism and investigate the role of the F and CT states as well as that of the vibronic interactions in the delocalization process.

The model commonly used to study electron transfer problems in conjunction with open quantum dynamics theory is one in which the electronic state is coupled to an intermediate harmonic oscillator and then to a heat-bath.[34] Then, a canonical transformation can be performed to incorporate the harmonic local modes into the bath, resulting in a multilevel system coupled to the heat bath by a Brownian spectral distribution (BSD) function.[35] Such a system can be treated using the HEOM formalism, in a numerically rigorous manner, even in the low-temperature case.[36,37] The HEOM can handle not only the strong system-bath coupling condition but also quantum coherence between the system and the bath that is important in the investigation of organic materials.[38,39]

In this work, we use Me-PTCDI (N,N′-dimethyl-3,4,9, 10-perylenedicarboximide) as a reference molecular system, which has been reported to have a particularly strong F–CT interaction.[40] We employ the HEOM approach for a BSD function to treat the Holstein model, which is further coupled to the heat-bath in order to explore the effect of the system parameters on the dynamics and on the spectral properties. We then show how the delocalization process affects the absorption and TGF spectra, providing information for analyzing the experimental results and hints for new possible studies.

The organization of this paper is as follows: In Sec. II, we present the HEOM for the Holstein Hamiltonian that includes F and CT states, the expressions of absorption and emission spectra, and the definition of the coherence length (N_{coh}). We then describe the model system in some detail. In Sec. III, we present the details of the calculation and the results of the simulation for various conditions. Section IV is devoted to concluding remarks.

II. THEORY

A. HEOM for a Holstein polaron model coupled to a bath

The HEOM for a Holstein–Pierls Hamiltonian was introduced in a previous study.[41] For this particular system, we consider the main contribution to be an electronic system linearly coupled to a local (Holstein) phonon mode which is further independently coupled to a harmonic oscillator heat-bath.

The total Hamiltonian is expressed in terms of the electronic Hamiltonian ($\hat{H}_{el}$), the electron–phonon interaction Hamiltonian ($\hat{H}_{el-ph}$) and the local phonon mode interaction with the heat-bath ($\hat{H}_{ph-B}$) as

$$\hat{H}_{tot} = \hat{H}_{el} + \hat{H}_{el-ph} + \hat{H}_{ph-B}. \tag{1}$$

The electronic Hamiltonian is then expressed in terms of the contribution of F states, CT states, and F–CT interaction as

$$\hat{H}_{el} = \hat{H}_F + \hat{H}_{CT} + \hat{H}_{F-CT}, \tag{2}$$

where each term is expressed as

$$\hat{H}_F = \sum_i \varepsilon_i^0 \hat{a}_i^\dagger \hat{a}_i + \sum_{i \neq j} t_{ij}^0 \hat{a}_i^\dagger \hat{a}_j, \tag{3}$$

$$\hat{H}_{CT} = \sum_m \varepsilon_m^0 \hat{a}_m^\dagger \hat{a}_m + \sum_{m \neq n} t_{mn}^0 \hat{a}_m^\dagger \hat{a}_n, \tag{4}$$

and

$$\hat{H}_{F-CT} = \sum_{mn \neq ij} t_{mn,ij}^0 \hat{a}_{mn}^\dagger \hat{a}_{ij}. \tag{5}$$

Here, $\hat{a}_i^\dagger$ ($\hat{a}_m^\dagger$) and $\hat{a}_i$ ($\hat{a}_m$) are the creation and annihilation operators, respectively, of the F excitons (CT) states. Moreover, ε_i^0 (ε_m^0) and t_{ij}^0 (t_{mn}^0) are the on-site electronic energy and the amplitude of the transfer integral for the i–jth F (m–nth CT) states. The term $t_{mn,ij}^0$ represents the F–CT interaction with $\hat{a}_{mn}^\dagger$ and $\hat{a}_{ij}$ being the creation and annihilation operator of the respective states.

The electron–phonon interaction Hamiltonian is given by

$$\hat{H}_{el-ph} = \sum_i \sum_\alpha \hat{V}_\alpha^i \left(\hat{b}_\alpha^\dagger + \hat{b}_\alpha \right) + \sum_m \sum_\alpha \hat{V}_\alpha^m \left(\hat{b}_\alpha^\dagger + \hat{b}_\alpha \right), \qquad (6)$$

with

$$\hat{V}_\alpha^i = \frac{1}{\sqrt{\mathcal{N}_C}} \hbar \Omega_\alpha g_i^\alpha \hat{a}_i^\dagger \hat{a}_i \qquad (7)$$

and

$$\hat{V}_\alpha^m = \frac{1}{\sqrt{\mathcal{N}_C}} \hbar \Omega_\alpha g_m^\alpha \hat{a}_m^\dagger \hat{a}_m, \qquad (8)$$

where the creation (annihilation) operator of the phonon (or vibron) mode α with frequency Ω_α is expressed as $\hat{b}_\alpha^\dagger$ ($\hat{b}_\alpha$). The local system–bath interactions are expressed as $\hat{V}_\alpha^i$ and $\hat{V}_\alpha^m$ for the F and CT terms, with the dimensionless coupling strength g_i^α and g_m^α, respectively. The constant $\mathcal{N}_C$ is the number of unit cells considered.

Finally, the phonon-bath Hamiltonian is expressed as

$$\hat{H}_{ph-B} = \sum_\alpha \hbar \Omega_\alpha \left(\hat{b}_\alpha^\dagger \hat{b}_\alpha + \frac{1}{2} \right) + \sum_{k=1}^N \hbar \omega_k \left(\hat{b}_k^\dagger \hat{b}_k + \frac{1}{2} \right)$$
$$+ \sum_\alpha \left(\hat{b}_\alpha^\dagger + \hat{b}_\alpha \right) \sum_{k=1}^N c_k^\alpha \left(\hat{b}_k^\dagger + \hat{b}_k \right), \qquad (9)$$

where the operator $\hat{b}_k^\dagger$ ($\hat{b}_k$) is the creation (annihilation) operator of the heat-bath phonons.

The bath system is modeled by a spectral distribution function (SDF), defined as

$$J_\alpha(\omega) \equiv \sum_{k=1}^N \left(c_k^\alpha \right)^2 \delta(\omega - \omega_k). \qquad (10)$$

For the heat-bath to be an unlimited heat source possessing an infinite heat capacity, the number of heat-bath oscillators N is effectively made infinitely large by replacing $J_\alpha(\omega)$ with a continuous distribution.

By using a canonical transformation, the Hamiltonian in Eq. (1) can be expressed in terms of the creation and annihilation operators of the heat-bath + primary oscillation ($\hat{b}_k'^\dagger$ and $\hat{b}_k'$, respectively) in the following general form:

$$\hat{H}_{tot} = \hat{H}_{el} + \sum_\alpha \sum_{k=1}^N \sum_i d_k^{ii\alpha} \hat{a}_i^\dagger \hat{a}_i (\hat{b}_k'^\dagger + \hat{b}_k') + \sum_{k=1}^N \hbar \omega_k \left(\hat{b}_k'^\dagger \hat{b}_k' + \frac{1}{2} \right), \quad (11)$$

where $d_k^{ii\alpha}$ is the dimensionless constant that represent the local interaction of the system with the oscillator-bath. Assuming the SDF of the later to be $J_\alpha(\omega) = \gamma_\alpha \omega$, we have the BSD defined as

$$J_\alpha'(\omega) = \frac{\hbar \lambda_\alpha}{2\pi} \frac{\gamma_\alpha \Omega_\alpha^2 \omega}{(\Omega_\alpha^2 - \omega^2)^2 + \gamma_\alpha^2 \omega^2}, \qquad (12)$$

where λ_α relates to the reorganization energy, which accounts for the displacement of the excited state in relation to the ground state in the oscillator coordinate space as a consequence of the local electron–phonon interaction. The parameter γ_α is the coupling strength between the oscillator and the bath, which is related to the peak width of $J_\alpha'(\omega)$.

The HEOM for the Brownian distribution can be expressed as

$$\frac{\partial}{\partial t} \hat{\rho}_{\{n^\alpha, m^\alpha; j_1^\alpha, \ldots, j_K^\alpha\}}(t) = -\left[\frac{i}{\hbar} \hat{H}_{el}^\times + \sum_\alpha \left\{ \frac{(n^\alpha + m^\alpha)}{2} \gamma_\alpha - i(n^\alpha - m^\alpha)\zeta_\alpha + \sum_{k=1}^K j_k^\alpha v_k^\alpha - \hat{\Xi}_\alpha \right\} \right] \hat{\rho}_{\{n^\alpha, m^\alpha; j_1^\alpha, \ldots, j_K^\alpha\}}(t)$$
$$+ \sum_\alpha \hat{V}_\alpha^\times \left[\hat{\rho}_{\{n^\alpha+1, m^\alpha; j_1^\alpha, \ldots, j_K^\alpha\}}(t) + \hat{\rho}_{\{n^\alpha, m^\alpha+1; j_1^\alpha, \ldots, j_K^\alpha\}}(t) \right]$$
$$+ \sum_\alpha n^\alpha \hat{\Theta}_-^\alpha \hat{\rho}_{\{n^\alpha-1, m^\alpha; j_1^\alpha, \ldots, j_K^\alpha\}}(t) + \sum_\alpha m^\alpha \hat{\Theta}_+^\alpha \hat{\rho}_{\{n^\alpha, m^\alpha-1; j_1^\alpha, \ldots, j_K^\alpha\}}(t)$$
$$+ \sum_\alpha \sum_{k=1}^K \hat{V}_\alpha^\times \hat{\rho}_{\{n^\alpha, m^\alpha; j_1^\alpha, \ldots, j_{k+1}^\alpha, \ldots, j_K^\alpha\}}(t) + \sum_\alpha \sum_{k=1}^K j_k^\alpha v_k^\alpha \hat{\Psi}_k^\alpha \hat{\rho}_{\{n^\alpha, m^\alpha; j_1^\alpha, \ldots, j_{k-1}^\alpha, \ldots, j_K^\alpha\}}(t), \qquad (13)$$

where the first term in brackets is the Liouvillian ($\hat{\mathscr{L}}^{(n,m)}$) that involves the truncation operator $\hat{\Xi}_\alpha$.[42] For a high number of hierarchical elements, the term $(n^\alpha + m^\alpha)\gamma_\alpha/2 + \sum_{k=1}^K j_k^\alpha v_k^\alpha$ becomes much larger than the characteristic time of the system. In this case, the hierarchy can be truncated by the terminator.[43]

B. Absorption and emission spectra

In optical measurements, a physical observable is expressed as an expectation value of a dipole operator evaluated from the density matrix $\hat{\rho}_{tot}(t)$ under laser excitations.[44] For example, linear

absorption is related to the first order response function expanded in terms of the laser interaction as

$$\hat{R}^{(1)}(t_1) = \frac{i}{\hbar} \langle [\hat{\mu}(t_1), \hat{\mu}(0)] \rangle$$
$$= \frac{i}{\hbar} \text{Tr} \left\{ \hat{\mu} e^{-i\hat{L}_{tot}^0 t_1} \hat{\mu}^\times \hat{\rho}_{tot}^{eq} \right\}, \qquad (14)$$

where ρ_{tot}^{eq} is the initial equilibrium state of the system, $\hat{\mu}$ is the total transition dipole operator, and $\hat{L}_{tot}^0$ is the Liouvillian operator of the system without the laser interaction. The time-evolution of the

density matrix elements after the pulse can be computed directly by employing the HEOM formalism described in Sec. II A. The intensity of the signal corresponding to the absorption spectrum is then obtained by performing the Fourier transform of the response function,

$$I_{Abs}(\omega) = \text{Im} \int_0^\infty dt R^{(1)}(t_1) e^{i\omega t}. \tag{15}$$

The third order response function is associated with nonlinear optical processes and is calculated for a sequence of four pulses as[45,46]

$$\hat{R}^{(3)}(t_3, t_2, t_1) = \frac{i}{\hbar^3} \langle [[[\hat{\mu}(t_1 + t_2 + t_3), \hat{\mu}(t_1 + t_2)], \hat{\mu}(t_1)], \hat{\mu}(0)] \rangle$$
$$= \frac{i}{\hbar^3} \text{Tr} \left\{ \hat{\mu} e^{-i\hat{L}_{tot}^0 t_3} \hat{\mu}^\times e^{-i\hat{L}_{tot}^0 t_2} \hat{\mu}^\times e^{-i\hat{L}_{tot}^0 t_1} \hat{\mu}^\times \hat{\rho}_{tot}^{eq} \right\}. \tag{16}$$

The design of the pulse sequence is what determines the formulation of the response function that can be associated with a specific spectroscopic technique. The first pulse creates coherence during the t_1 period and the second pulse creates an optical excitation of the system. In pump–probe spectroscopy both the spontaneous emission (SE) from the excited states and the Raman from the ground state contribute to the overall signal. However, if we assume instant excitation, i.e., $t_1 = 0$, the excitation and gate pulses do not overlap and one can neglect resonant Raman scattering contributions. We can then compute the time-gated fluorescence (TGF) signal (or the SE signal) that consists only of the fluorescence of the excited state component at different times (t^*). Employing the HEOM approach, we can simulate the TGF spectrum to obtain information on the wavepacket dynamics as well as ultrafast excited state relaxation that arises from nonadiabatic processes, which will be helpful to conduct and analyze experiments.[31,32,47,48] The SE signal is expressed as

$$S_{SE}(t^*, \omega) = \text{Re} \int_0^\infty dt_3 \int_0^\infty dt_2 R^{(3)}(t_3, t_2, 0) E_G(t_2 - t^*)$$
$$\times E_G(t_2 + t_3 - t^*) e^{i\omega t_3}. \tag{17}$$

Here, E_G is the intensity of the time-gate pulse, which is assumed to have the following Gaussian shape:

$$E_G(t_2 - t^*) E_G(t_2 + t_3 - t^*) = \exp \left\{ \left[\frac{t_2 - t^*}{t_G} \right]^2 + \left[\frac{t_2 + t_3 - t^*}{t_G} \right]^2 \right\}, \tag{18}$$

where t_G is the so-called time-gate and controls the time resolution of the TGF signal. By integrating the HEOM, we can evaluate $R^{(3)}(t_3, t_2, 0)$ as functions of t_2 and t_3.[43] The TGF spectrum is then obtained by performing a Fourier transform on t_3.

C. Coherence length

The coherence length (N_{coh}) is a widely employed parameter to evaluate the degree of exciton delocalization. Here, we consider the definition expressed as[49,50]

$$N_{coh}(t) = \frac{1}{|C(t,0)|} \sum_i |C(t,i)|, \tag{19}$$

where

$$C(t,i) = \text{Tr} \left[\sum_j \hat{a}_i^\dagger \hat{a}_j \rho^{(2)}(t,0) \right], \tag{20}$$

and $C(t,i)$ is often referred to as the coherence field, and depends on the specific molecular site, while $\rho^{(2)}(t,0)$ is the on-site density matrix after the two laser excitations. We point out that other definitions of N_{coh} exist, although they appear to be less common.[51]

Spano has been the first to investigate the possibility to determine the N_{coh} from spectroscopic measurements[19,20,30] and suggested to use the approximate relation

$$N_{coh}(t) \approx \lambda^2 \frac{I^{0-0}(t)}{I^{0-1}(t)}, \tag{21}$$

where I^{0-0} and I^{0-1} are the intensities of the 0–0 and 0–1 emission peaks of the fluorescence spectra, and λ^2 is the Huang–Rhys factor. Note that, although this expression has been used for both J- and H-aggregates,[29] the theoretical justification was mainly focused on J-aggregates. In the following, we will show that the above relation has several limitations and that it may lead to erroneous results when applied to H-aggregates.

III. RESULTS AND DISCUSSION

In the present study, we simulate the exciton transfer process in a PBI dimer using a four-level system comprising two excited F states $|F_1\rangle$ and $|F_2\rangle$, and two CT states $|CT_1\rangle$ and $|CT_2\rangle$ (2F-2CT model), as illustrated in Fig. 1.[52] In this model, each state is coupled to its own local vibrational mode, which is further coupled to the heat bath. We consider the frequency and the coupling strength of the vibrational modes to be identical for the two F states, but different coupling strengths for the two CT states. Moreover, we assume that there is no interaction between the CT states. For comparison, we simulate the dynamics of a PBI tetramer including only a single F state (4F model), a dimer ignoring CT states (2F model), and a monomer (1F model).

The model Hamiltonian for the 2F-2CT electric states is expressed in matrix form as

$$\hat{H}_{el} = \hbar \begin{bmatrix} \omega_{F_1} & \Delta_{12} & \Delta_e & \Delta_h \\ \Delta_{21} & \omega_{F_2} & \Delta_h & \Delta_e \\ \Delta_e & \Delta_h & \omega_{CT_1} & 0 \\ \Delta_h & \Delta_e & 0 & \omega_{CT_2} \end{bmatrix}, \tag{22}$$

where $\hbar\omega_i$ is the F exciton (CT) energy of the ith (mth) state associated with ε_i (ε_m) and $\hbar\Delta_{ij}$ ($\hbar\Delta_{ij}$) is the coupling strength between the
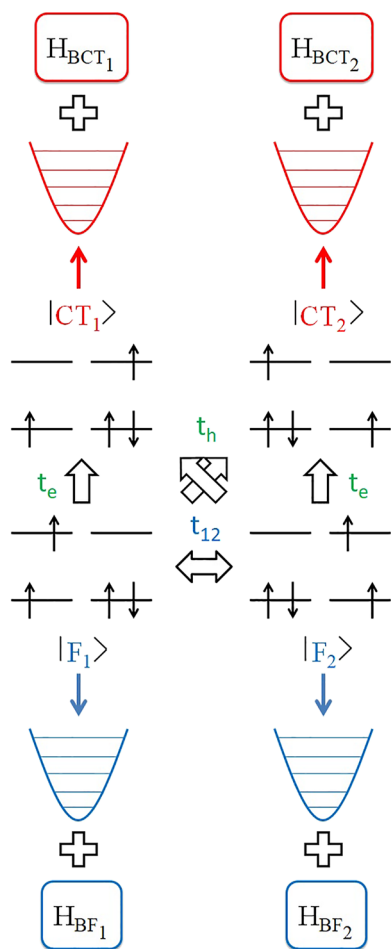
FIG. 1. Schematic view of the F-CT model described by the Hamiltonian in Eqs. (1)–(8) for a four-level system. Each state is coupled to its own local vibrational mode and to the local bath.

ith and jth (mth and nth) states associated with the transfer integral t_{ij} (F–CT interaction t_{mn}).

The parameters adopted in the present study have been derived from literature data, and are loosely based on the Me-PTCDI molecule.[40] However, to investigate the role of the F-CT state interaction on the dynamic behavior of the model system, we varied the system parameters, as described below.

For all of our computations, we set the energy of the F states as $\omega_{F_1} = \omega_{F_2} = 0$ and consider the room temperature case ($T = 300$ K) with the value of $\beta\hbar\omega = 2.40$. Although the bandgap (E_{gap}) energy between F and CT states will be changed later, we start with the CT energy as $\omega_{CT_3} = \omega_{CT_4} = 480$ cm^{-1}. The off-diagonal elements representing the interaction between excited states are $\Delta_{12} = \Delta_{21} = 500$ cm^{-1}. For the F–CT interaction parameters, we set the electron transfer integrals to $\Delta_e = -725$ cm^{-1}, and the hole transfer integrals to $\Delta_h = -160$ cm^{-1}.[40] As mentioned earlier, we assume that there is no interaction between the CT states. For

the pure excitonic case, i.e., the 2F and 4F models, the transfer parameters are set under the nearest-neighbor condition.

In the following, the effect of the coupling between the vibrational subsystem and its environment is described by the Brownian oscillator model. The vibrational modes of F and CT states are described as $\Omega_{F_1} = \Omega_{F_2} = \Omega_{CT_1} = \Omega_{CT_2} = 1400$ cm^{-1} with coupling strength $\lambda_{F_1} = \lambda_{F_2} = 1200$ cm^{-1}, $\lambda_{CT_1} = 850$ cm^{-1}, and $\lambda_{CT_2} = 465$ cm^{-1}. The coupling strength between the local oscillator and the bath, which acts as the inverse noise correlation time of the BSD, is set to $\gamma \equiv \gamma_\alpha = 500$ cm^{-1} for $\alpha = F_1, F_2, CT_1$, and CT_2, respectively. These values are chosen to reproduce the width of the vibronic peaks in the experimental absorption spectra. We consider the molecular units to be independent and all the thermal baths to be uncorrelated. To provide a simple dynamic picture of and CT transfer processes, we assume that only one molecule is initially excited ($\rho_{F_1}(0) = 1$). We simulate the time evolution of the reduced density matrix by numerically integrating the HEOM with respect to the time using the fourth-order Runge-Kutta method. The depth and the truncation number of hierarchy are chosen to $N = 10$ with $K = 2$.

Then, all spectroscopic signals of the aggregate are computed assuming that only the $|F_1\rangle$ and $|F_2\rangle$ states are bright, that is,

$$\hat{\mu} = |g\rangle\langle F_1| + |g\rangle\langle F_2| + \text{H.c.,} \qquad (23)$$

where $|g\rangle$ is the ground electronic state of the system. In general, the CT states are dark and have little or no transition dipoles, so they can be safely ignored.

A. Population dynamics

The time-evolution of the reduced density matrix elements for the 2F, 4F, and 2F-2CT models is depicted in Figs. 2(a)–2(c), respectively. We simulate the dynamics up to $t = 210$ fs, which is sufficient to reach the equilibrium state under these conditions. We observe an ultrafast temporal evolution in the range of 50 fs, followed by thermalization. As it can be seen from the CT dynamics results, the population of the $|CT_1\rangle$ state increases rapidly in a short time, whereas the population ratio with the $|CT_2\rangle$ state reverses at a long time. This is because the absolute value of the transfer integral between the $|F_1\rangle$ and $|CT_1\rangle$ states is almost five times larger than the value of the hole transfer integral between the $|F_1\rangle$ and $|CT_2\rangle$ states, allowing the fast interconversion. However, the coupling to the local vibrational mode is about twice as large in the $|CT_1\rangle$ state than the $|CT_2\rangle$ state, which means that the relaxation is stronger at longer times, resulting in a population inversion. The effect of the electron and hole transfer integral parameters are illustrated in the supplementary material (see Fig. S1).

Note that the value of γ was chosen to reproduce the bandwidth of the absorption spectra; however, this leads to an underestimation of the relaxation times in comparison to experimental values on analogous perylene aggregate systems.[29] Therefore, we suggest that the broadening of the absorption peaks observed in the experimental spectra of these aggregates is very likely related to static inhomogeneity rather than dynamic bath effects. These effects could be easily incorporated into the current HEOM formalism by including Gaussian fluctuations set by an infinite correlation time (i.e.,
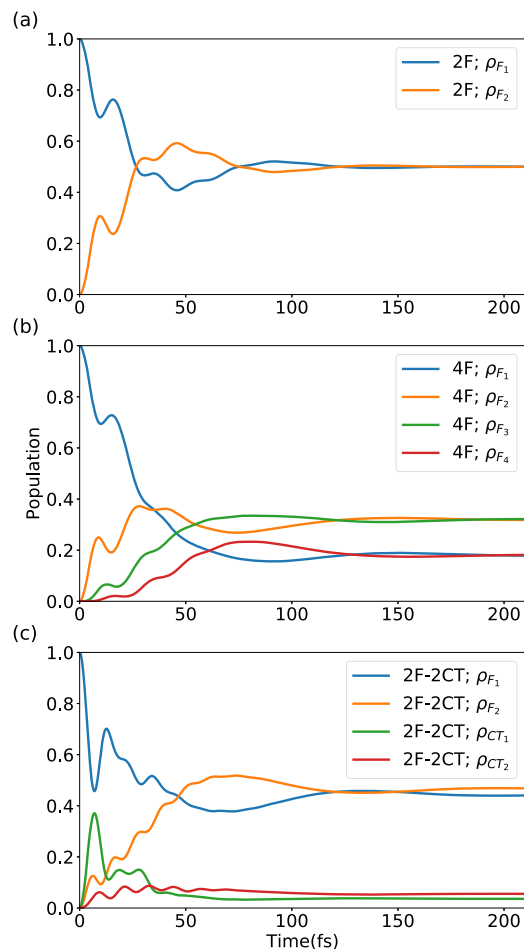
FIG. 2. Time-evolution of the density matrix elements for the (a) 2F, (b) 4F, and (c) 2F-2CT models.

FIG. 3. Absorption spectra for the (a) 1F, 2F, 4F, and 2F-2CT models, and absorption spectra for the (b) 2F-2CT model with various values of E_{gap} between the F and CT states.

$\gamma = 0$).[43,53] However, for the sake of simplicity, such an analysis is not performed here.

B. Absorption spectra

Figure 3(a) depicts the absorption spectra of the 1F, 2F, 4F, and 2F-2CT models. Here, the vibronic absorption peaks are designated as A_{ν}, where ν is an integer number. In the case of the 1F model, the peaks represent the excitations from a ground-state vibrational mode to an F-electron state vibrational mode, described by high frequency displaced harmonic oscillators. In the case of the aggregates, however, the mechanism by which the peaks arise is more complex. We observe the A_1 peak at around 1200 cm^{-1} and the A_2 and A_3 peaks in the pure F state models. The difference in frequency between the absorption peaks of the 1F model corresponds to the value of the local mode ($\Omega_{\alpha} = 1400$ cm^{-1}) and is increased by the effect of the transfer integral in the 2F and 4F models.

As the number of sites increases, the overall spectrum is blue-shifted with a decrease in the A_1 peak intensity and an increase in
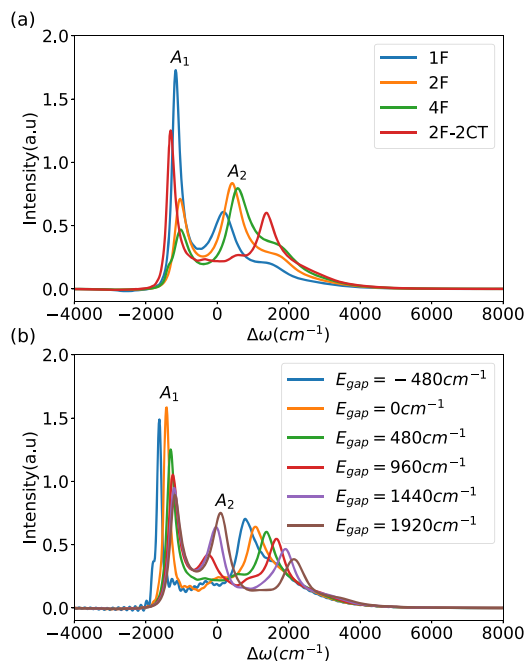
the A_2 intensity. This behavior is expected for oligomers and it is attributed to the π–π stacking of PBIs molecules in H-aggregates.[54] However, in the 2F-2CT system, the A_1 peak is observed to be red-shifted and stronger in comparison to the 2F model. The presence of a second peak near 1500 cm^{-1} is also confirmed. The high-frequency peak is a consequence of the influence of the CT states.[55] Absorption peaks of the two F states and the peak due to the CT states are overlapped. The frequency difference between the main peak and the high-frequency peak is related to the effect of the electron and hole transfer integrals, which produces the split and the overall red-shift of the two F states part of the spectrum. The detailed analysis is presented in the supplementary material (see Fig. S2). We noted the presence of similar interaction mechanisms in many push–pull chromophores and showed that the relevance of the CT state affects the position and intensity of the vibronic bands.[56]

The effect of the bandgap was reported previously[57] and is illustrated in Fig. 3(b). As the energy difference between the F and CT states increases, the presence of the A_1 peak and high-frequency peak suppress gradually. An increase in the intensity of the A_2 peak and an overall blue shift in the spectrum are also observed. This behavior can be easily understood by considering that by increasing E_{gap}, the CT states are decoupled from the F states and their effect on the absorption spectrum is reduced.

C. TGF spectra

The TGF measurement can provide detailed information on the interaction between oscillatory dynamics and delocalization in PBI aggregates. This technique describes the stimulated emission
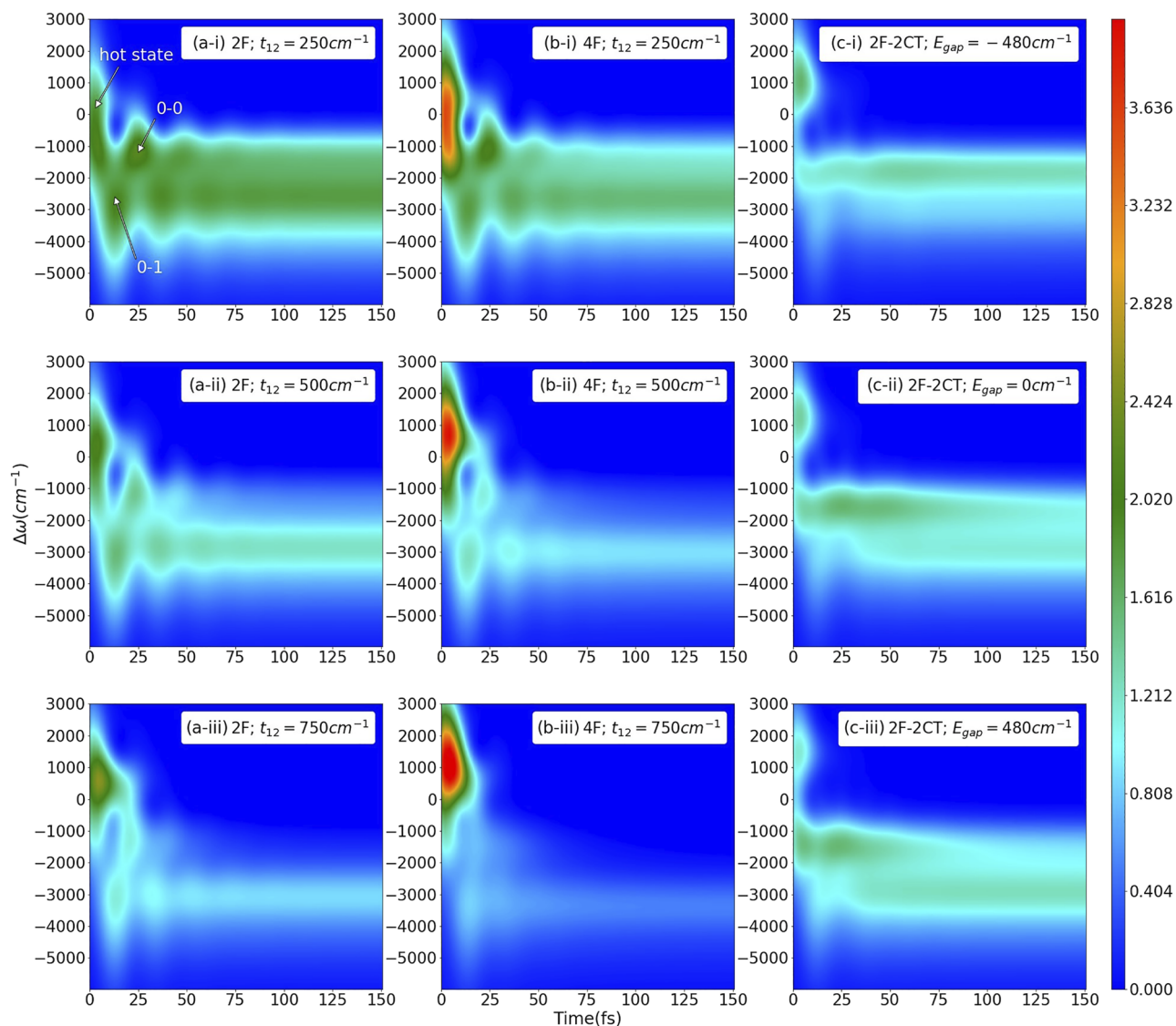
FIG. 4. TGF spectra (t_G = 10 fs) of the (a) 2F and (b) 4F models for (i)–(iii) different values of t_{12}, and of the (c) 2F-2CT model for (i)–(iii) different values of E_{gap} between F and CT states for t_{12} = 500 cm^{-1}.

spectrum as a function of time after excitation, allowing direct mapping of the dynamics of the excited state. The TGF spectra results for t_G = 10 fs are depicted in Fig. 4 for the 2F [(a-i)–(a-iii)] and 4F [(b-i)–(b-iii)] models for various values of t_{12}, and for the 2F-2CT [(c-i)–(c-iii)] model for various values of E_{gap} between F and CT states with t_{12} = 500 cm^{-1}.

All results exhibit a sharp band in the positive frequency region at very short times (<10 fs), which rapidly decays and disappears completely at longer times. Since we assume an instantaneous (Franck–Condon type) excitation from the ground electronic state to the F states, the origin of this signal is clearly related to the

emission from highly localized hot vibronic states created after the initial photoexcitation. Because of the fast relaxation (i.e., large γ), the excited wave packet relaxes to the ground state very quickly and the signal disappears. As observed in the absorption spectra, the position of the hot peak is blue-shifted with increasing t_{12} and E_{gap} due to the effect of molecular stacking, resulting in a split of the emission peak.

After this very short initial phase, two time-periodic peaks were observed at about −1200 and −2600 cm^{-1}, respectively. We notice that the energy difference between the peaks corresponds to the frequency of the local Brownian mode (Ω_α = 1400 cm^{-1}). Furthermore,
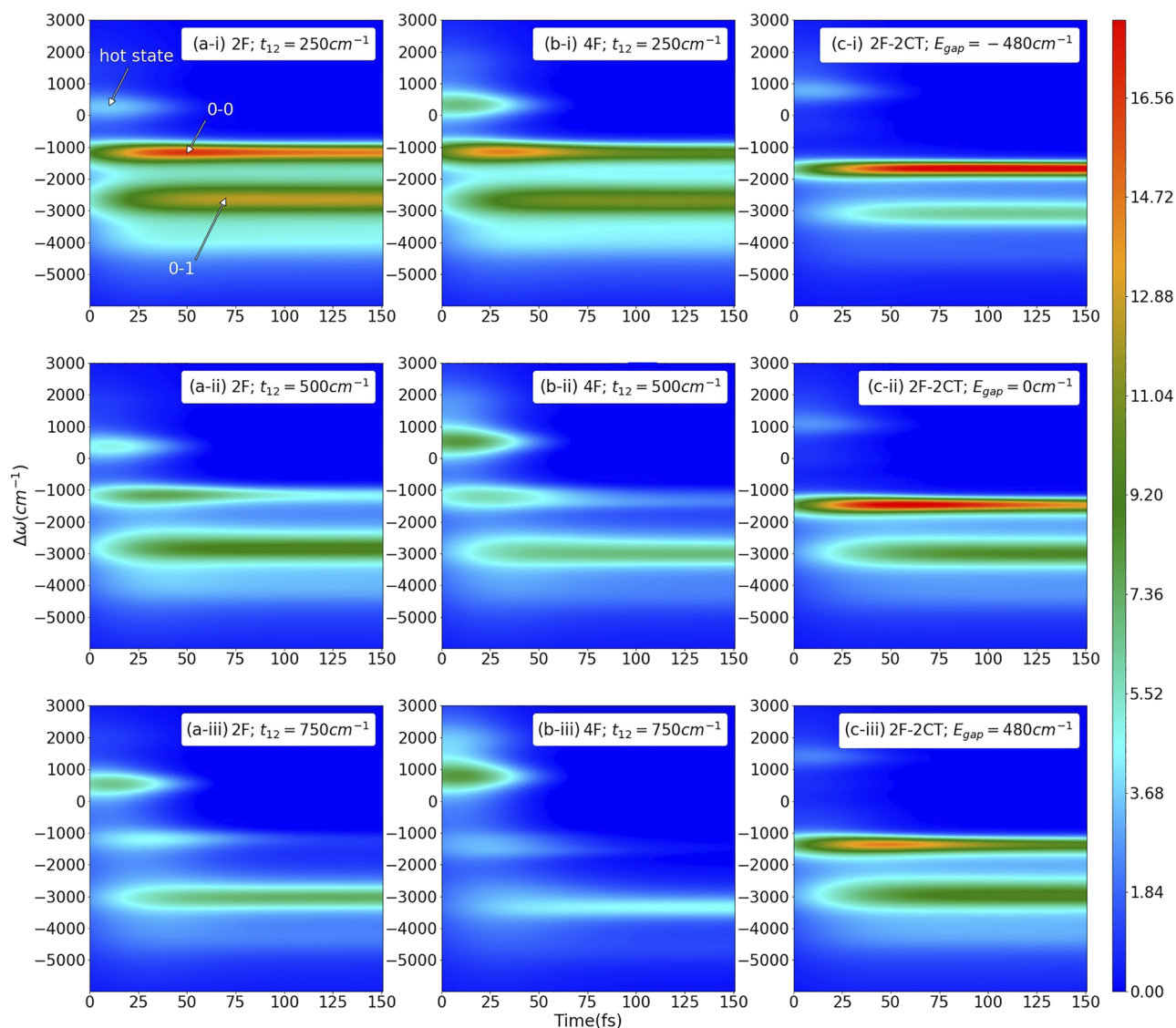
FIG. 5. TGF spectra (t_G = 50 fs) of the (a) 2F and (b) 4F models for (i)–(iii) different values of t_{12} and of the (c) 2F-2CT model for (i)–(iii) different values of E_{gap} between F and CT states for t_{12} = 500 cm^{-1}.

the intensities of the two peaks oscillate at a frequency of about 24 fs, which is also in agreement with the period of the Brownian mode ($1/\Omega_\alpha$). The oscillations span a time range of about 100 fs and slowly transform into a stationary pattern around 150 fs. The stationary signal corresponds to the steady state fluorescence spectrum of the aggregate. The calculated results obtained for the oligomers for a time-gate of t_G = 50 fs are depicted in Figs. 5(a)–5(c).

In the 2F model [see Figs. 5(a-i)–5(a-ii)], we can easily assign the hot state, 0–0 and 0–1 emission peaks,[20] although the position and the splitting of the peaks increase with the number of states and with higher values of t_{12}. We observe that the initial intensity of the

0–0 emission peak becomes weaker and decays faster with increasing values of t_{12}. The inclusion of CT states strongly affects the TGF spectrum. The TGF spectra of the 2F-2CT model [Figs. 5(c-i)–5(c-ii)] show that the intensity of the hot state peak is reduced and its position shifted in comparison to the 2F model having the same value of t_{12} [Fig. 5(a-ii)]. Moreover, the intensity of the 0–0 peak is increased, and the intensity of the 0–1 peak is reduced. This effect becomes more pronounced with decreasing E_{gap}. Due to the selection of a large time-gate, fast wave packet motion cannot be observed and its oscillatory features are averaged out. The intensity of the emission peak at very short times is greatly reduced because

the relaxation process is comparable to the time-gate. Experimental results showing similar features have recently been reported in the literature.[29]

The short t_G used in Fig. 4, on the other hand, allows us to clearly see how the wave packet moves from the initially excited hot state to the 0–0 emission peak and then to the 0–1 emission peak. As mentioned above, such characteristics are specified by the frequency of the local mode and are independent of other system-bath parameters. Given the complexity of these models, this is a surprisingly simple result, valid for a wide range of system parameters. However, when the exciton or F-CT coupling is very large, this simple pattern no longer holds.

It is important to mention that the TGF signal reported here shows some significant differences from the results obtained with approximate methods.[30] The first is the appearance of a strong peak in a very short period of time. The second is that the intensity of the 0–1 peak at −2600 cm^{-1} is initially zero and increases with time, whereas it was previously reported to be nearly constant. This clearly demonstrates the importance of using an adequate model with the accurate treatment of the vibrational relaxation process in the computation of nonlinear spectral signals.

D. Coherent length

According to the modern theory of molecular aggregates, the extent of exciton delocalization in J- and H-aggregates, measured by N_{coh} as defined in Eq. (19), reflects in the ratio of the intensity of the 0–0 and 0–1 peaks of the luminescence spectra.[20] More specifically for H-aggregates, the larger N_{coh}, the higher is the intensity of the 0–1 peak with respect to the 0–0 peak. Recently, it has been shown that the approximate relation given in Eq. (21) can provide reliable information about the delocalization extent in J-aggregates, and might work for H-aggregates only on a very short time scale, while being unreliable at long times.[30] On the other hand, Sung *et al.* have used the same relation combined with the measurement of TGF spectra to describe the dynamics of delocalization in H-aggregates of PBI units.[29] Due to this controversial issue, we have calculated N_{coh} defined by Eq. (19) for the 2 sites (2F and 2F-2CT models) and the 4 site (4F model) systems and compared them to the approximate value obtained from Eq. (21) using the computed TGF spectra. Figure 6 shows the results of the time-evolution of N_{coh} based on Eq. (19) (colored lines) and Eq. (21) (dotted lines) of the 2F and 4F models with different values of t_{12} (a,b) and of the 2F-2CT model for different values of E_{gap} for t_{12} = 500 cm^{-1} (c).

We notice that, in all cases, the delocalized exciton created after the initial photoexcitation tends to localize at very short times due to the motion of the vibrational wavepacket. After the transient localization, N_{coh} reaches a constant value. It is also evident that the limiting values increase with increasing t_{12} and E_{gap}. The results of the 2F-2CT model clearly evidence that, for the set of parameters used, the transient exciton localization is enhanced when CT states are included. In some previous studies, CT states have been described as an intermediate state that promotes localization via excimer formation.[58]

Equation (21) can be readily employed from the intensities of the 0–0 and 0–1 peaks of the TGF spectra. The results, obtained for a Huang–Rhys factor of λ^2 = 0.734, are notably different in comparison to the theoretical definition of Eq. (19). More specifically, up
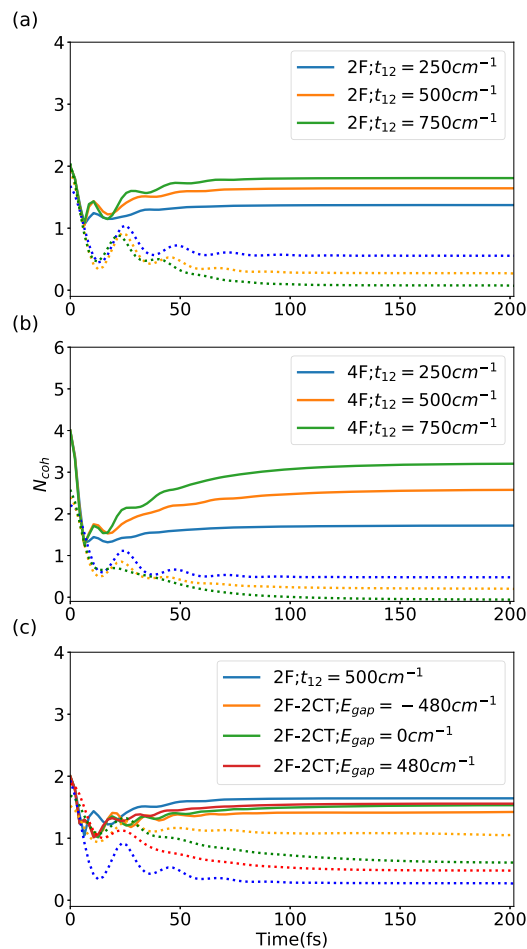

FIG. 6. Time-evolution of N_{coh} using Eq. (19) (color lines) and Eq. (21) (dotted lines) for the (a) 2F and (b) 4F models for different values of t_{12}, and for the (c) 2F-2CT model for different values of E_{gap} between F and CT states for t_{12} = 500 cm^{-1}.

to a few tens of femtoseconds N_{coh} reproduces the theoretical value; however, it falls very rapidly to values smaller than 1 that are clearly unphysical. We notice that this estimate is obtained for a specific t_G. In order to observe the initial oscillatory behavior, t_G must be sufficiently small. However, since the experimental lower limit of t_G is about 50 fs, the actual observation of the transient behavior may be difficult (see Fig. S3 in the supplementary material). Furthermore, while the limiting value of N_{coh} should clearly increase with increasing t_{12} (greater delocalization), the estimate obtained from the TGF spectra provides the opposite behavior.

The above analysis clearly suggest that the estimate of N_{coh} provided by Eq. (21) cannot be adopted for the study of H-aggregate dynamics as it provided physically unreliable results.

IV. CONCLUSION

The effect of mixing F-CT states in H-aggregates was investigated using the HEOM method for the Holstein polaron model.

The dynamics and spectroscopic properties of the model with the Me-PTCDI derivative as a reference were investigated. The role of the vibronic interactions and of the F–CT interaction states in the exciton delocalization process was analyzed by varying the strength of the F–CT interaction. The calculated absorption spectra were consistent with previous results.[19,20] In general, compared to models that only include F states, those that include CT states caused (i) a redshift of the spectrum; (ii) an increase and decrease in the intensity of the A_1 and A_2 peaks, respectively; and (iii) the appearance of high frequency peaks as a result of splitting caused by the F–CT interaction.

Although technical limitations preclude experimental observation at this time, TGF calculations predicted the existence of ultrafast exciton dynamics that depend only on the frequency of the local bath (high frequency molecular mode). Furthermore, we observed the appearance of an excited hot state peak whose intensity is strongly correlated with the initial exciton delocalization, and that decays with a constant time that depends on the relaxation time of the system. Finally, all our calculations indicated that the F–CT interaction promotes exciton localization, manifested in the decrease in intensity of the hot state and 0–0 peaks and the increase in intensity of the 0–1 peak, resulting in a decrease of N_{coh}.

However, when the value of N_{coh} was calculated using a simplified formula based on the intensities of the peaks of the TGF spectra, the results were unphysical, and one should be cautious about using it in the case of H-aggregates.

In order to increase the size of the model used in this study, it is important to reduce the numerical cost of HEOM. Recently, efficient algorithms based on tensor-train representations of reduced density matrices have been developed and are expected to be applied to HEOM for more realistic systems,[59–64] although its stability and numerical accuracy have not yet been established.[65,66]

SUPPLEMENTARY MATERIAL

See the supplementary material for the effect of t_e and t_h in the time-evolution of the density matrix elements and in the absorption spectra for the 2F-2CT model system. The time-evolution of N_{coh} employing Eq. (21) for different values of t_G is also shown for the 2F, 4F, and 2F-2CT models.

AUTHOR DECLARATIONS

Conflict of Interest

The authors have no conflicts to disclose.

Author Contributions

Mauro Cainelli: Conceptualization (lead); Data curation (lead); Formal analysis (equal); Investigation (lead); Methodology (equal); Software (lead); Writing – original draft (lead). **Raffaele Borrelli**: Conceptualization (lead); Formal analysis (equal); Investigation (equal); Project administration (equal); Writing – review & editing (equal). **Yoshitaka Tanimura**: Funding acquisition (lead); Investigation (equal); Methodology (lead); Project administration (equal); Resources (lead); Writing – review & editing (equal).

DATA AVAILABILITY

The data that support the findings of this study are available from the corresponding authors upon reasonable request.

REFERENCES

[1] G. Horowitz, "Organic field-effect transistors," Adv. Mater. **10**, 365–377 (1998).

[2] C. D. Dimitrakopoulos and P. R. L. Malenfant, "Organic thin film transistors for large area electronics," Adv. Mater. **14**, 99–117 (2002).

[3] J. Zhang, H. S. Tan, X. Guo, A. Facchetti, and H. Yan, "Material insights and challenges for non-fullerene organic solar cells based on small molecular acceptors," Nat. Energy **3**, 720–731 (2018).

[4] K. Sato, J. Mizuguchi, Y. Sakai, and S. Aramaki, "Crystal structure of parallel-stacked peryleneimides and their application to organic field-effect transistor devices," J. Appl. Phys. **103**, 013702 (2008).

[5] C. Li, J. H. Yum, S. J. Moon, A. Herrmann, F. Eickemeyer, N. G. Pschirer, P. Erk, J. Schöneboom, K. Müllen, M. Grätzel, and M. K. Nazeeruddin, "An improved perylene sensitizer for solar cell applications," ChemSusChem **1**, 615–618 (2008).

[6] U. Gómez, M. Leonhardt, H. Port, and H. C. Wolf, "Optical properties of amorphous ultrathin films of perylene derivatives," Chem. Phys. Lett. **268**, 1–6 (1997).

[7] J. Mizuguchi and K. Tojo, "Electronic structure of perylene pigments as viewed from the crystal structure and excitonic interactions," J. Phys. Chem. B **106**, 767–772 (2002).

[8] Z. G. Soos, M. H. Hennessy, and G. Wen, "Frenkel and charge transfer states of conjugated polymers and molecules," Chem. Phys. **227**, 19–32 (1998).

[9] M. H. Hennessy, Z. G. Soos, R. A. Pascal, and A. Girlando, "Vibronic structure of PTCDA stacks: The exciton phonon-charge-transfer dimer," Chem. Phys. **245**, 199–212 (1999).

[10] T. Fujita, S. Atahan-Evrenk, N. P. D. Sawaya, and A. Aspuru-Guzik, "Coherent dynamics of mixed Frenkel and charge-transfer excitons in dinaphtho[2,3-*b*:2′3′-*f*]thieno[3,2-*b*]thiophene thin films: The importance of hole delocalization," J. Phys. Chem. Lett. **7**, 1374–1380 (2016).

[11] W. Popp, M. Polkehn, K. H. Hughes, R. Martinazzo, and I. Burghardt, "Vibronic coupling models for donor-acceptor aggregates using an effective-mode scheme: Application to mixed Frenkel and charge-transfer excitons in oligothiophene aggregates," J. Chem. Phys. **150**, 244114 (2019).

[12] S. Jiang, Y. Xie, and Z. Lan, "The role of the charge-transfer states in the ultrafast excitonic dynamics of the DTDCTB dimers embedded in a crystal environment," Chem. Phys. **515**, 603–613 (2018).

[13] M. Hoffmann and Z. G. Soos, "Optical absorption spectra of the Holstein molecular crystal for weak and intermediate electronic coupling," Phys. Rev. B **66**, 024305 (2002).

[14] M. Hoffmann, K. Schmidt, T. Fritz, T. Hasche, V. M. Agranovich, and K. Leo, "The lowest energy Frenkel and charge-transfer excitons in quasi-one-dimensional structures: Application to MePTCDI and PTCDA crystals," Chem. Phys. **258**, 73–96 (2000).

[15] J.-L. Brédas, J. E. Norton, J. Cornil, and V. Coropceanu, "Molecular understanding of organic solar cells: The challenges," Acc. Chem. Res. **42**, 1691–1699 (2009).

[16] S. Kang, C. Kaufmann, Y. Hong et al, "Ultrafast coherent exciton dynamics in size controlled perylene bisimide aggregates," Struct. Dyn. **6**, 064501 (2019).

[17] C. Kaufmann, W. Kim, A. Nowak-Król, Y. Hong, D. Kim, and F. Würthner, "Ultrafast exciton delocalization, localization, and excimer formation dynamics in a highly defined perylene bisimide quadruple π-stack," J. Am. Chem. Soc. **140**, 4253–4258 (2018).

[18] W. Poppa, M. Polkehn, R. Binder, and I. Burghardt, "Coherent charge transfer exciton formation in regioregular P3HT: A quantum dynamical study," J. Phys. Chem. Lett. **10**, 3326–3332 (2019).

[19] N. J. Hestand and F. C. Spano, "Expanded theory of H- and J-molecular aggregates: The effects of vibronic coupling and intermolecular charge transfer," Chem. Rev. **118**, 7069–7163 (2018).

[20] F. C. Spano, "Excitons in conjugated oligomer aggregates, films, and crystals," Annu. Rev. Phys. Chem. **57**, 217–243 (2006).

[21] K. Sun, X. Liu, W. Hu, M. Zhang, G. Long, and Y. Zhao, "Singlet fission dynamics and optical spectra of pentacene and its derivatives," Phys. Chem. Chem. Phys. **23**, 12654–12667 (2021).

[22] K. Sun and Y. Zhao, "Beating maps of singlet fission: Simulation of coherent two-dimensional electronic spectroscopy by Davydov ansatz in organic molecules," J. Chem. Phys. **147**, 224905 (2017).

[23] G. Yang, N. Wu, T. Chen, K. Sun, and Y. Zhao, "Theoretical examination of long-range energy propagation in nano-engineered light-harvesting antenna arrays," J. Phys. Chem. C **116**, 3747–3756 (2012).

[24] F. Zheng, L. Chen, J. Gao, and Y. Zhao, "Fully quantum modeling of exciton diffusion in mesoscale light harvesting systems," Materials **14**, 3291 (2021).

[25] T. Meier, Y. Zhao, V. Chernyak, and S. Mukamel, "Polarons, localization, and excitonic coherence in superradiance of biological antenna complexes," J. Chem. Phys. **107**, 3876 (1997).

[26] Y. Zhao, T. Meier, W. M. Zhang, V. Chernyak, and S. Mukamel, "Superradiance coherence sizes in single-molecule spectroscopy of LH2 antenna complexes," J. Phys. Chem. B **103**, 3954–3962 (1999).

[27] F. C. Spano, J. Clark, C. Silva et al., "Determining exciton coherence from the photoluminescence spectral line shape in poly(3-hexylthiophene) thin films," J. Chem. Phys. **130**, 074904 (2009).

[28] F. C. Spano and H. Yamagata, "Vibronic coupling in J-aggregates and beyond: A direct means of determining the exciton coherence length from the photoluminescence spectrum," J. Phys. Chem. B **115**, 5133–5143 (2011).

[29] J. Sung, P. Kim, B. Fimmel, F. Würthner, and D. Kim, "Direct observation of ultrafast coherent exciton dynamics in helical π-stacks of self-assembled perylene bisimides," Nat. Commun. **6**, 8646 (2015).

[30] R. Tempelaar, F. C. Spano, J. Knoester, and T. L. C. Jansen, "Mapping the evolution of spatial exciton coherence through time-resolved fluorescence," J. Phys. Chem. Lett. **5**, 1505–1510 (2014).

[31] M. F. Gelin, A. V. Pisliakov, and W. Domcke, "Time- and frequency-gated spontaneous emission as a tool for studying vibrational dynamics in the excited state," Phys. Rev. A **65**, 062507 (2002).

[32] M. F. Gelin and R. Borrelli, "Simulation of nonlinear femtosecond signals at finite temperature via a thermo field dynamics-tensor train method: General theory and application to time- and frequency-resolved fluorescence of the Fenna–Matthews–Olson complex," J. Chem. Theory Comput. **17**, 4316 (2021).

[33] M. F. Gelin, D. Egorova, and W. Domcke, "Efficient calculation of time- and frequency-resolved four-wave-mixing signals," Acc. Chem. Res. **42**, 1290–1298 (2009).

[34] Y. Tanimura and S. Mukamel, "Optical Stark spectroscopy of a Brownian oscillator in intense fields," J. Phys. Soc. Jpn. **63**, 66–77 (1994).

[35] M. Tanaka and Y. Tanimura, "Quantum dissipative dynamics of electron transfer reaction system: Nonperturbative hierarchy equations approach," J. Phys. Soc. Jpn. **78**, 073802 (2009).

[36] X. Xie, A. Santana-Bonilla, and A. Troisi, "Nonlocal electron–phonon coupling in prototypical molecular semiconductors from first principles," J. Chem. Theory Comput. **14**, 3752–3762 (2018).

[37] K. Nakamura and Y. Tanimura, "Optical response of laser-driven charge-transfer complex described by Holstein-Hubbard model coupled to heat baths: Hierarchical equations of motion approach," J. Chem. Phys. **155**, 064106 (2021).

[38] A. A. Bakulin, A. Rao, V. G. Pavelyev, P. H. M. van Loosdrecht, M. S. Pshenichnikov, D. Niedzialek, J. Cornil, D. Beljonne, and R. H. Friend, "The role of driving energy and delocalized states for charge separation in organic semiconductors," Science **335**, 1340–1344 (2012).

[39] S. Gélinas, A. Rao, A. Kumar, S. L. Smith, A. W. Chin, J. Clark, T. S. van der Poll, G. C. Bazan, and R. H. Friend, "Ultrafast long-range charge separation in organic semiconductor photovoltaic diodes," Science **343**, 512–516 (2014).

[40] L. Gisslén and R. Scholz, "Crystallochromy of perylene pigments: Interference between Frenkel excitons and charge-transfer states," Phys. Rev. B **80**, 115309 (2009).

[41] M. Cainelli and Y. Tanimura, "Exciton transfer in organic photovoltaic cells: A role of local and nonlocal electron–phonon interactions in a donor domain," J. Chem. Phys. **154**, 034107 (2021).

[42] A. Ishizaki and Y. Tanimura, "Quantum dynamics of system strongly coupled to low-temperature colored noise bath: Reduced hierarchy equations approach," J. Phys. Soc. Jpn. **74**, 3131–3134 (2005).

[43] Y. Tanimura, "Stochastic Liouville, Langevin, Fokker–Planck, and master equation approaches to quantum dissipative systems," J. Phys. Soc. Jpn. **75**, 082001 (2006).

[44] S. Mukamel, Y. Tanimura, and P. Hamm, "Coherent multidimensional optical spectroscopy," Acc. Chem. Res. **42**, 1207–1209 (2009).

[45] Y. Tanimura, "Numerically 'exact' approach to open quantum dynamics: The hierarchical equations of motion (HEOM)," J. Chem. Phys. **153**, 020901 (2020).

[46] Y. Tanimura and A. Ishizaki, "Modeling, calculating, and analyzing multidimensional vibrational spectroscopies," Acc. Chem. Res. **42**, 1270–1279 (2009).

[47] L. Chen, M. F. Gelin, Y. Zhao, and W. Domcke, "Mapping of wave packet dynamics at conical intersections by time- and frequency-resolved fluorescence spectroscopy: A computational study," J. Phys. Chem. Lett. **10**, 5873–5880 (2019).

[48] L. Chen, R. Borrelli, D. V. Shalashilin, Y. Zhao, and M. F. Gelin, "Simulation of time- and frequency-resolved four-wave-mixing signals at finite temperatures: A thermo-field dynamics approach," J. Chem. Theory Comput. **17**, 4359 (2021).

[49] O. Kühn and V. Sundström, "Pump–probe spectroscopy of dissipative energy transfer dynamics in photosynthetic antenna complexes: A density matrix approach," J. Chem. Phys. **107**, 4154 (1997).

[50] T. Meier, V. Chernyak, and S. Mukamel, "Multiple exciton coherence sizes in photosynthetic antenna complexes viewed by pump-probe spectroscopy," J. Phys. Chem. B **101**, 7332–7342 (1997).

[51] C. Smyth, F. Fassioli, and G. D. Scholes, "Measures and implications of electronic coherence in photosynthetic light-harvesting," Philos. Trans. R. Soc., A **370**, 3728–3749 (2012).

[52] A. G. Dijkstra and Y. Tanimura, "Linear and third- and fifth-order nonlinear spectroscopies of a charge transfer system coupled to an underdamped vibration," J. Chem. Phys. **142**, 212423 (2015).

[53] M. F. Gelin, A. Velardo, and R. Borrelli, "Efficient quantum dynamics simulations of complex molecular systems: A unified treatment of dynamic and static disorder," J. Chem. Phys. **155**, 134102 (2021).

[54] C. Shao, M. Grüne, M. Stolte, and F. Würthner, "Perylene bisimide dimer aggregates: Fundamental insights into self-assembly by NMR and UV/Vis spectroscopy," Chem. Eur. J. **18**, 13665–13677 (2012).

[55] N. J. Hestand and F. C. Spano, "Molecular aggregate photophysics beyond the kasha model: Novel design principles for organic materials," Acc. Chem. Res. **50**, 341–350 (2017).

[56] A. Capobianco, R. Borrelli, A. Landi, A. Velardo, and A. Peluso, "Absorption band shapes of a push–pull dye approaching the cyanine limit: A challenging case for first principle calculations," J. Phys. Chem. A **120**, 5581–5589 (2016).

[57] N. J. Hestand, R. V. Kazantsev, A. S. Weingarten, L. C. Palmer, S. I. Stupp, and F. C. Spano, "Extended-charge-transfer excitons in crystalline supramolecular photocatalytic scaffolds," J. Am. Chem. Soc. **138**, 11762–11774 (2016).

[58] S. Kang, T. Kim, Y. Hong, F. Würthner, and D. Kim, "Charge-delocalized state and coherent vibrational dynamics in rigid PBI H-aggregates," J. Am. Chem. Soc. **143**, 9825–9833 (2021).

[59] R. Borrelli, "Density matrix dynamics in twin-formulation: An efficient methodology based on tensor-train representation of reduced equations of motion," J. Chem. Phys. **150**, 234102 (2019).

[60] R. Borrelli and S. Dolgov, "Expanding the range of hierarchical equations of motion by tensor-train implementation," J. Phys. Chem. B **125**, 5397–5407 (2021).

[61] Y. Ke, R. Borrelli, and M. Thoss, "Hierarchical equations of motion approach to hybrid fermionic and bosonic environments: Matrix product state formulation in twin space," J. Chem. Phys. **156**, 194102 (2022).

[62] R. Borrelli and M. F. Gelin, "Finite temperature quantum dynamics of complex systems: Integrating thermo-field theories and tensor-train methods," WIREs Comput. Mol. Sci. **11**, e1539 (2021).

[63] Q. Shi, Y. Xu, Y. Yan, and M. Xu, "Efficient propagation of the hierarchical equations of motion using the matrix product state method," J. Chem. Phys. **148**, 174102 (2018).

[64] Y. Yan, T. Xing, and Q. Shi, "A new method to improve the numerical stability of the hierarchical equations of motion for discrete harmonic oscillator modes," J. Chem. Phys. **153**, 204109 (2020).

[65] R. Borrelli and M. F. Gelin, "Quantum electron-vibrational dynamics at finite temperature: Thermo field dynamics approach," J. Chem. Phys. **145**, 224101 (2016).

[66] R. Borrelli and M. F. Gelin, "Simulation of quantum dynamics of excitonic systems at finite temperature: An efficient method based on thermo field dynamics," Sci. Rep. **7**, 9127 (2017).